PHILOSOPHICAL TRANSACTIONS OF THE ROYAL SOCIETY B BIOLOGICAL SCIENCES

Diffuse Neutron Scattering from Crystal Imperfections [and Discussion]

E. W. J. Mitchell, R. J. Stewart, R. J. R. Miller and D. J. Cebula

Phil. Trans. R. Soc. Lond. B 1980 **290**, 511-526
doi: 10.1098/rstb.1980.0112

Phil. Trans. R. Soc. Lond. B **290**, 511–526 (1980)
Printed in Great Britain

Diffuse neutron scattering from crystal imperfections

By E. W. J. Mitchell† and R. J. Stewart‡
† *The Clarendon Laboratory, Oxford OX1 3PU, U.K.*
‡ *J. J. Thomson Physical Laboratory,*
The University, Whiteknights, Reading RG6 2AF, U.K.

The most extensively studied type of structural diffuse scattering in recent years has been the small angle scattering centred on 000. Examples are given illustrating the types of investigation that can now be made: precipitation in alloys (*in situ* kinetic studies); fracture of alloys (*in situ* mechanical studies); radiation 'damage' in silicon (correlation with spectroscopic measurements); radiation damage in gallium arsenide (anisotropic effects).

In comparison with small angle neutron scattering, much less work has been done on other types of diffuse scattering. Some possible developments in this field are indicated by the computer simulation of relaxation effects around impurity atoms.

Introduction

Crystal imperfections constitute departures from the perfect periodicity of the ideal crystal and therefore give rise to diffuse scattering, i.e. scattering of radiation of wavelengths and at angles other than those given by the Bragg relation. The application of neutrons to the study of imperfections through diffuse scattering has a number of complementary advantages compared with X-rays or electrons.

One of the most important of these is the much greater penetration of neutrons, which allows thick samples to be used and, especially, allows much longer wavelengths to be used. The thickness for 10% absorption at 1 Å† for neutrons is commonly 1–100 cm compared with 5×10^{-4} to 1×10^{-3} cm for X-rays. Indeed, with neutrons it is fairly routine to use wavelengths of 10 Å such that only diffuse scattering occurs and that Bragg and double Bragg scattering are completely eliminated. This is particularly important for small-angle scattering in which, by using smaller wavelengths, the intensities may be seriously affected by double Bragg scattering. In the study of diffuse scattering, advantage may also be taken of one of the general characteristics of the nuclear scattering of neutrons, that the scattering lengths (b) for nuclei of adjacent atomic number can be quite different, whereas for X-rays they are similar. Advantage of this may be taken in studies of materials such as AlMg, AlMgSi or NiFe alloys. The ability to use long wavelength neutrons has the further advantage that because of their low energy (1 meV), phonon emission processes cannot occur, so that the only thermal diffuse scattering possible arises from phonon absorption, which may be effectively eliminated by cooling.

Early measurements of diffuse scattering, either by the total or the differential cross section, were hampered by lack of intensity. The field has, however, developed substantially in recent years through the use of beams from the High Flux Reactor at the Institut Laue–Langevin (I.L.L.) in Grenoble. For small-angle scattering the impact of the I.L.L. has allowed experiments to be done that were previously quite impossible.

† 1 Å = 10^{-10} m = 10^{-1} nm.

It is convenient to consider three régimes of diffuse scattering, although the division is to some extent arbitrary:

(*a*) *small angle scattering*, scattering in the vicinity of the reciprocal lattice point (000) produced by relatively large fluctuations in scattering length density;

(*b*) *diffuse scattering*, between Bragg peaks and between the lowest angle Bragg peak and the straight through beam, produced by strain around defects especially from the relatively large displacements in the first few shells of atoms around the defect;

(*c*) *Huang scattering*, close to Bragg peaks and difficult to separate quantitatively, produced especially by the long-range part of the strain field around defects.

The requirement to work near Bragg peaks in Huang scattering means that there is no general advantage in using neutrons in that case and we shall not discuss Huang scattering in the present paper.

In this paper we give examples of small-angle neutron scattering (s.a.n.s.) obtained by ourselves and collaborators. The examples illustrate two aspects of s.a.n.s. work: (i) obtaining information about the size and shape of inhomogeneities in crystals, and (ii) using s.a.n.s. to characterize inhomogeneities and to follow their changes with time under various conditions. We then discuss the problem of determining the strain field around point defects, or small complexes, by a combination of diffuse scattering measurements and the computer simulation of models of the displacements of the surrounding atoms.

2. Experimental

(*a*) *Principles*

Scattering conditions are described by completing the scattering triangle in reciprocal space. All information about the disorder is contained in the disorder structure factor, $S(Q)$, between reciprocal lattice points, and this has to be determined experimentally. In s.a.n.s. one is determining $S(Q)$ in the vicinity of (000), although similar information is contained around other reciprocal lattice points. However, by working with long wavelengths we eliminate double Bragg scattering processes, which also produce contributions to the intensity at small angles. Our problem, therefore, is to map out the intensity by using scattering triangles within the first set of reciprocal lattice points.

The experiments reported here were performed at the I.L.L. with the instrument D11 which covers both the small-angle range, corresponding to $5 \times 10^{-4} < Q < 5 \times 10^{-1}$ Å^{-1}, and also, with the new counter bank, the range $0.3 < Q < 3$ Å^{-1}. The wavelengths available are from 4.5 to 20 Å. This means that $S(Q)$ may be continuously sampled within the volume of the first Brillouin zone without moving the specimen.

(*b*) *Instrumental*

There are currently about ten spectrometers throughout the world suitable for diffuse neutron scattering studies, including two recently commissioned in the U.K. specifically for the small Q region: the Pluto S.A.S. at Harwell and the Herald S.A.S. at Aldermaston.

For work requiring the highest sensitivity in the small Q region, however, D11 at the I.L.L. is by far the best instrument available for all disciplines, so that the time available for a given experiment is severely limited.

PHILOSOPHICAL TRANSACTIONS OF THE ROYAL SOCIETY B BIOLOGICAL SCIENCES

D11 has been described fully by Ibel (1976). Neutrons from a cold source, which enhances the long wavelength part of the spectrum, are transmitted through 60 m of curved guide tube into an experimental hall. Being remote from the reactor, this hall has a low background. The wavelength spread ($\Delta\lambda$) in the beam is then limited by a helical velocity selector of resolution ($\Delta\lambda/\lambda$) of 9%. The transmitted wavelength can be varied within the range $4.5 \leqslant \lambda \leqslant 20$ Å by varying the rotational velocity of the selector. The beam then passes through a series of guides and/or apertures which allows the angular divergence to be varied. Thus a collimated beam of long wavelength neutrons is produced. Neutrons scattered by the sample are detected by two arrays of detectors: the small-angle multi-detector and the high-angle detector bank.

The small-angle detector is a $^{10}BF_3$ (1 atm) proportional counter giving a two-dimensional sensitivity by incorporating a multiwire array. It provides 3808 active elements each of 1 cm^2 spread over a square of 64 cm × 64 cm. The detector can be placed at several distances between 1 and 40 m from the sample, giving an angular range of 18–0.15°. At the centre of the array there is a cadmium beam stop to absorb the unscattered beam.

The high-angle bank, which was installed in 1977, comprises 32 ^{3}He proportional counters, each having a sensitive area of 30 cm × 2.5 cm, arranged at angles between 20 and 140° from the beam line and with constant Q increments. Unlike the small-angle counter, the high-angle bank covers only one portion of the azimuth. Each counter is provided with a collimator to avoid counting stray neutrons.

The entire neutron path from the velocity selector to the detectors is enclosed by one vacuum chamber 80 m long, which is evacuated to 10^{-2} Torr (*ca.* 1.33 Pa) to reduce air scattering.

Finally, we refer to the diffuse scattering spectrometer, which a group associated with one of us (Stewart 1978) has designed for the Spallation Neutron Source. By an ingenious arrangement of movable, annular, position-sensitive detectors the azimuth is fully covered for $10^{-3} \leqslant Q \leqslant 3$ Å^{-1}. Use of the time-of-flight method means that all required wavelengths can be sampled concurrently and that double Bragg scattering and inelastic effects may be discriminated against.

Instrumentally, therefore, the present and future is healthy and we give in the following sections an account of some of the results that we have obtained, together with an indication of future possibilities.

3. Small-angle neutron scattering

(*a*) *Theory*

The theory of small-angle scattering has been reviewed by many authors (e.g. Guinier & Fournet 1955) from various points of view. We give here the essential results for our discussion.

S.a.n.s. arises from fluctuations in the scattering length density $c(\boldsymbol{r})$ associated with a number density of nuclei $\rho(\boldsymbol{r})$. The scattering cross section is given by

$$\mathrm{d}\sigma/\mathrm{d}\Omega = |\mathscr{F}\{c(\boldsymbol{r})\}|^2, \tag{1}$$

where $\mathscr{F}$ denotes the Fourier transform. We are especially interested in applying this to an inhomogeneity ($c(\boldsymbol{r}) = c_\mathrm{i}(\boldsymbol{r})$) in an otherwise homogeneous matrix ($c(\boldsymbol{r}) = c_\mathrm{m}$). For a particle of shape $g(\boldsymbol{r}-\boldsymbol{r}_0)$, such that $g_\mathrm{i} = 1$ for $\boldsymbol{r}-\boldsymbol{r}_0 < \boldsymbol{r}_\mathrm{i}$ and 0 for $\boldsymbol{r}-\boldsymbol{r}_0 > \boldsymbol{r}_\mathrm{i}$, where $\boldsymbol{r}_\mathrm{i}$ denotes the boundary measured from the centre of the inhomogeneity $\boldsymbol{r}_0$, we can write

$$c(\boldsymbol{r}) = c_\mathrm{m}\{1-g(\boldsymbol{r}-\boldsymbol{r}_0)\}+c_\mathrm{i}(\boldsymbol{r})\cdot g(\boldsymbol{r}-\boldsymbol{r}_0).$$

PHILOSOPHICAL TRANSACTIONS OF THE ROYAL SOCIETY B BIOLOGICAL SCIENCES

It follows that $$\mathrm{d}\sigma/\mathrm{d}\Omega = (\bar{c}_\mathrm{i} - c_\mathrm{m})^2 \, |\mathscr{F}\{g(\boldsymbol{r}-\boldsymbol{r}_0)\}|^2, \tag{2}$$

where $$\bar{c}_\mathrm{i} = \frac{1}{V_\mathrm{i}} \int_{r_\mathrm{i}} c_\mathrm{i}(\boldsymbol{r}) \cdot \mathrm{d}^3\boldsymbol{r}, \tag{3}$$

in which V_i is the volume of the inhomogeneity. It is clear from (2) that unless there is a compositional change (different combination of the scattering lengths – b's) or a local macroscopic density change, the s.a.n.s. will be zero.

We may write $\bar{c}_\mathrm{i}$ as $$\bar{c}_\mathrm{i} = \frac{1}{V_\mathrm{i}} \int_{r_\mathrm{i}} (\rho_{\mathrm{ia}}(\boldsymbol{r}) \cdot b_\mathrm{a} + \rho_{\mathrm{ib}}(\boldsymbol{r}) \cdot b_\mathrm{b}) \, \mathrm{d}^3\boldsymbol{r}$$

for a diatomic system, or for one species

$$\bar{c}_\mathrm{i} = \frac{b}{V_\mathrm{i}} \int_{r_\mathrm{i}} \rho_\mathrm{i}(\boldsymbol{r}) \cdot \mathrm{d}^3\boldsymbol{r}.$$

The method of moments may then be applied to the $\mathscr{F}\{g(\boldsymbol{r}-\boldsymbol{r}_0)\}$ in (2) and various combinations of the observed quantities used to calculate characteristic lengths (first moment), areas (second) or volumes (third). Ideally, the observed ratios between these quantities give information about the shape of the particle by comparison with ratios calculated for particular shapes.

The well known equations derived by Guinier (Guinier & Fournet 1955) and Porod (1951) effectively use this approach. For low concentrations N_i (cm^{-3}) of identical, randomly orientated inhomogeneities, the Guinier approximation equation (2) becomes

$$\frac{\mathrm{d}\sigma}{\mathrm{d}\Omega} = N_\mathrm{i}(\bar{c}_\mathrm{i} - c_\mathrm{m})^2 \, V_\mathrm{i}^2 \, \mathrm{e}^{-\frac{1}{3}Q^2R_\mathrm{g}^2}, \tag{4}$$

where R_g^2 is the second moment given by

$$R_\mathrm{g}^2 = \int_{r_\mathrm{i}} \rho(\boldsymbol{r}) \cdot \boldsymbol{r}^2 \, \mathrm{d}^3\boldsymbol{r} \Big/ \int_{r_\mathrm{i}} \rho(\boldsymbol{r}) \cdot \mathrm{d}^3\boldsymbol{r}, \tag{5}$$

and in the special case of spheres (R_s), $R_\mathrm{g} = (\frac{3}{5})^{\frac{1}{2}} R_\mathrm{s}$. In Porod's approximation, the cross section is evaluated to the $(QR)^2$ term in the sine expansion, and within that limit the cross section for large Q becomes

$$\frac{\mathrm{d}\sigma}{\mathrm{d}\Omega} = N_\mathrm{i}(\bar{c}_\mathrm{i} - c_\mathrm{m})^2 \frac{2\pi}{Q^4} A_\mathrm{i}, \tag{6}$$

where A_i is the surface area of an inhomogeneity. These equations apply to polycrystalline samples and can be used only indirectly to give information about the shape of an inhomogeneity.

More direct information about the shape of the inhomogeneities may be obtained from single crystal measurements. In this case, non-spherical inhomogeneities may be aligned along a few equivalent crystallographic directions and produce anisotropic scattering. This may be calculated by summing over these equivalent directions so that

$$\frac{\mathrm{d}\sigma}{\mathrm{d}\Omega} = N_\mathrm{i}(\bar{c}_\mathrm{i} - c_\mathrm{m})^2 \sum_{\langle hkl \rangle} \left| \int_{r_\mathrm{i}} g(\boldsymbol{r}-\boldsymbol{r}_0) \cdot \mathrm{e}^{\mathrm{i}\boldsymbol{Q}\cdot\boldsymbol{r}} \, \mathrm{d}^3\boldsymbol{r} \right|^2. \tag{7}$$

For higher concentrations such that interference between the particles has to be included, (2) becomes

$$\frac{\mathrm{d}\sigma}{\mathrm{d}\Omega} = N_\mathrm{i}(\bar{c}_\mathrm{i} - c_\mathrm{m})^2 \, |\mathscr{F}\{g(\boldsymbol{r}-\boldsymbol{r}_0)\}|^2 \left[\frac{1}{N_\mathrm{i}} \sum_{ij}^{\infty} \mathrm{e}^{\mathrm{i}\boldsymbol{Q}\cdot(\boldsymbol{r}_{0\mathrm{i}} - \boldsymbol{r}_{0\mathrm{j}})} \right], \tag{8}$$

PHILOSOPHICAL TRANSACTIONS OF THE ROYAL SOCIETY B BIOLOGICAL SCIENCES

where $\boldsymbol{r}_{0i}$ and $\boldsymbol{r}_{0j}$ are the centres of the inhomogeneities i and j. For widely spaced inhomogeneities the term in the square bracket (the interference term) is 1; for higher concentrations it oscillates but the first maximum is the only one that need be considered.

For randomly distributed inhomogeneities the interference term becomes

$$\{1-\phi(Q,d)\} \quad \text{with} \quad \phi(Q,d) = 3(\sin Qd - Qd\cos Qd)/(Qd)^3,$$

and a maximum occurs in curves of $\mathrm{d}\sigma/\mathrm{d}\Omega$ against Q, at

$$Q_{\max}\, d = 5.76. \tag{9}$$

for example, $d = 100$ Å, $Q_{\max} = 5.76 \times 10^{-2}$ Å^{-1}. In all cases, the presence of a size distribution of the inhomogeneities may smear out the maximum in the scattering cross section.

(*b*) *Application to alloys*

(i) *Introduction*

The strength of alloys is generally improved by the development of a second phase dispersed throughout the host matrix, often in the form of a precipitate. The strengthening is influenced by factors such as the size distribution of the particles, their concentration and their coherence with the matrix. These factors contribute to diffuse scattering, especially in the low Q region, and by using neutrons we can study thick samples.

(ii) *Aluminium–zinc alloys*

From previous work (see, for example, Kostorz 1979) it appears that the decomposition phase, produced by ageing at relatively low temperatures after quenching from relatively high ones, consists of more or less spherical Zn-rich precipitates. Gerold (1961) has interpreted the X-ray data as indicating spherical precipitates of a single composition, with the observed scattering peak related to interparticle interference. On the other hand, Guinier (1959) has suggested that the effects arise from an inner Zn-rich zone surrounded concentrically by an outer Zn-depleted region.

There are two processes by which such precipitates may be formed: spinodal decomposition, and nucleation followed by growth. The thermodynamic data about the spinodal line are sparse and there have been attempts to use other data to uniquely assign one or other mode of decomposition. Much of our early work was in an attempt to resolve these problems (Allen *et al.* 1976).

The object of the further experiments that are described here was to follow the decomposition process '*in situ*' on D 11 and to see whether the subsequent dissolution process could be similarly followed. A special high-temperature cell was built for incorporation into the beam line; this has been described by Allen (1978).

In earlier experiments, Messoloras (1974) and Allen *et al.* (1976) found that for compositions of 4.5, 6.7 and 11.8 at. % Zn there were two regions of precipitate growth. The initial fast region was over in $t \leqslant 100$ min, whereas in the second stage growth occurred indefinitely, although slowly. The transition between the régimes was found to be independent of the Zn concentration but was a function of the homogenization temperature (T_Q) from which the samples were quenched.

Results from an '*in situ*' experiment are shown in figure 1. Those measurements by Allen (1978) were all for the 11.8 at. % Zn alloy and are given for growth temperatures, T_g, of 110

PHILOSOPHICAL TRANSACTIONS OF THE ROYAL SOCIETY B BIOLOGICAL SCIENCES

and 175 °C. T_Q was 300 °C in all cases. Growth temperatures were studied for $100 < T_g < 200$ °C.

The development of the small-angle scattering can clearly be followed: the whole set of curves was obtained in 76 min for $T_g = 110$ °C and 220 min for 175 °C. Guinier plots gave for the end of this initial growth $R_g \approx 34$ Å for $T_g = 110$ °C and 90 Å for 175 °C. From the position of the maxima, and using (4), we find the 34 Å precipitates were separated on average by *ca.* 260 Å while the larger precipitates were *ca.* 770 Å apart. We were thus able to follow the production of well separated larger particles at the higher growth temperature, compared with the closer (260 Å) smaller (34 Å) particles produced at 110 °C.

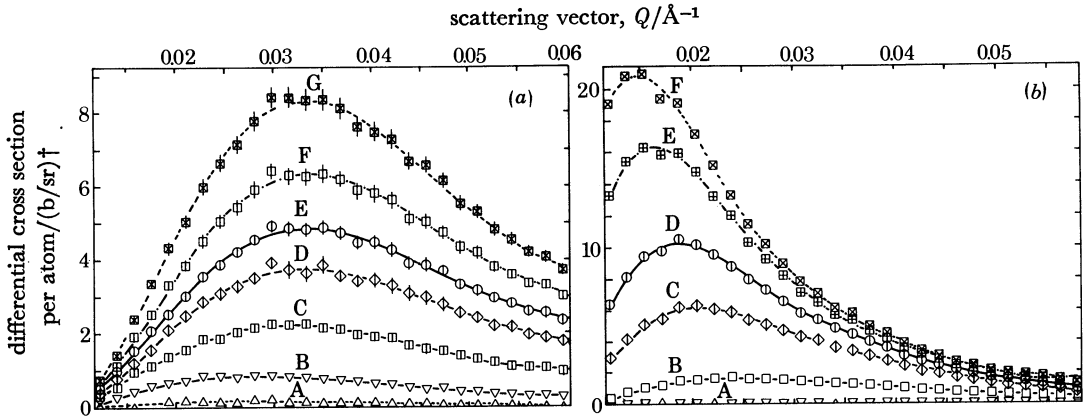

FIGURE 1. Decomposition of an Al–11.8 at. % Zn alloy. (*a*) Ageing temperature 110 °C; ageing times in minutes: A, 20; B, 27; C, 34; D, 40; E, 46; F, 56; G, 76. (*b*) Ageing temperature 175 °C; ageing times in minutes: A, 18; B, 39; C, 71; D, 104; E, 163; F, 220. † 1 barn (b) = 10^{-28} m^2.

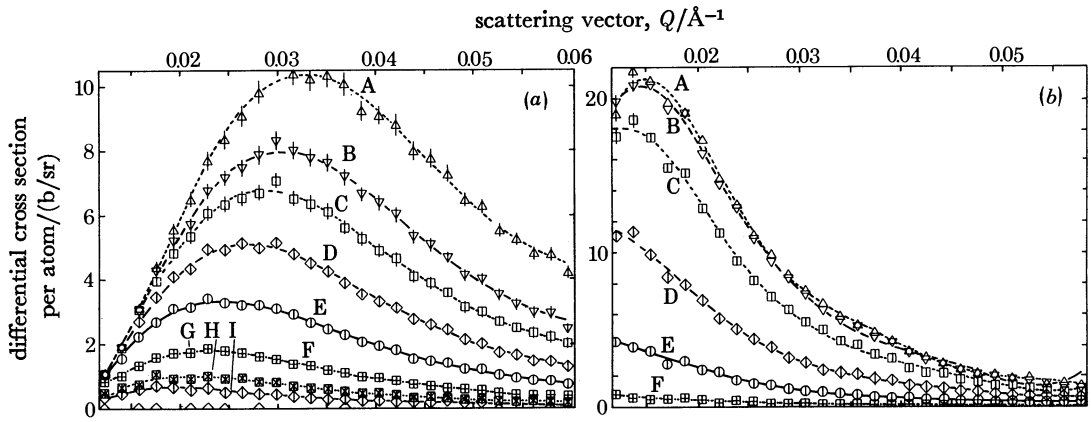

FIGURE 2. Dissolution at 300 °C of an Al–11.8 at. % Zn alloy. (*a*) Following growth at 110 °C, dissolution times in minutes: A, 0; B, 4.5; C, 7; D, 9; E, 11.5; F, 13.5; G, 16; H, 18; I, 21. (*b*) Following growth at 175 °C, dissolution times in minutes: A, 0; B, 0.6; C, 1.7; D, 2.8; E, 4.0; F, 5.1.

In figure 2 we show the effect of heating to 300 °C on the precipitates produced under the two growth conditions discussed above. This is the homogenization temperature, and the dissolution of the precipitates – the decrease of the small-angle neutron scattering – is clearly shown. For the sample aged at 175 °C the dissolution was followed and was complete in 7 min. We conclude from these experiments that faster dissolution is associated with higher T_g and

therefore that large, widely spaced particles dissolve more rapidly than smaller, more closely packed ones.

We are not able to present a full kinetic analysis here, but the experiments show that such processes may now be readily followed by neutron scattering. We have discussed elsewhere (Allen *et al.* 1978) the reasons why the above conclusion seems to eliminate intra-particle diffusion as the limiting process in the dissolution.

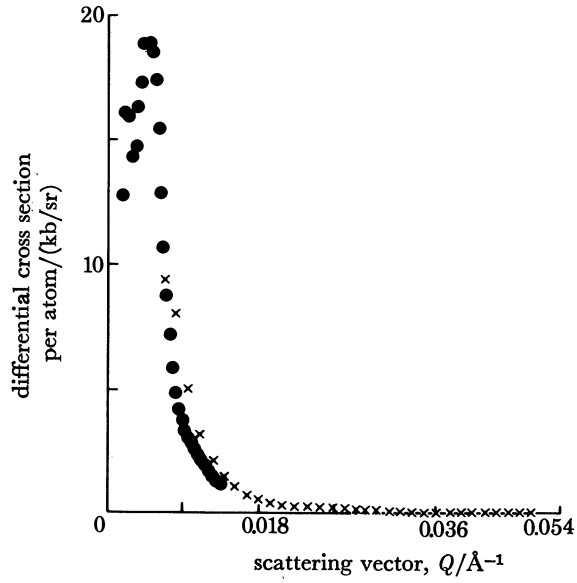

FIGURE 3. Small-angle scattering curve for a Nimonic 105 alloy. Combined 20 m and 5 m sample-detector measurements on D11.

(iii) *Nickel-based 'super-alloys'*

These alloys are composed primarily of Ni, Co, Cr, Mo, Al and Ti. Because of their resistance to creep at high temperatures, they are extensively used in high temperature–stress applications. The resistance to creep is believed to be associated with the size, distribution and concentration of a precipitated phase (the γ' phase). This phase is an ordered alloy having an f.c.c. structure of the form $(NiCo)_3(AlTi)$. The particular alloy examined in the experiments reported here, Nimonic 105, has the atomic composition 52Ni, 20Co, 15Cr, 4Mo, 8Al, 1Ti.

In spite of the good high-temperature creep-resistant properties of these alloys, continuous use at high temperatures and stresses leads to a degradation. It has been suggested that Ostwald ripening of the precipitates is the cause of the degradation, i.e. the dissolution of small precipitates in the vicinity of large ones, which then become larger. The atomic numbers of the main constituents are Al, 12; Ti, 22; Cr, 23; Co, 26; Ni, 27 such that there is relatively low discrimination of the γ' phase in X-ray scattering. The neutron scattering lengths are: Al, 0.35; Ti, −0.34; Cr, 0.35; Co, 0.25; Ni, 1.03. Rearrangement of the Ni, Co, Al, Cr and Ti concentrations therefore gives rise to substantial fluctuations in neutron scattering length density.

Two sets of experiments were carried out, one in which the scattering was measured after an ageing (strengthening) heat treatment and the second in which the scattering was followed dynamically in a high-temperature creep experiment. The latter was carried out in the neutron beam of D11 in a specially designed cell described by Miller *et al.* (1978).

PHILOSOPHICAL TRANSACTIONS OF THE ROYAL SOCIETY B BIOLOGICAL SCIENCES

For the first experiment the alloy was homogenized by heating at 1150 °C for 16 h and then aged for 16 h at 850 °C. The s.a.n.s. is shown in figure 3. Preliminary analysis showed that in the expected Guinier region the $\ln(d\sigma/d\Omega)$–Q^2 plots were curved, and Miller *et al.* (1978) have used the distribution discussed by Shull & Roess (1947) to derive the distribution of particle sizes. The mean size found was $\bar{R}_g = 300$ Å and hence $\bar{R}_s = 390$ Å.

The sample was then heated for $7\frac{1}{2}$ h at 750 °C under a uniaxial stress of 300 MPa and it was found that Q_{max} has decreased and $\bar{R}_g$ increased by 15%. The increase in both D and $\bar{R}_g$ indicates that some particles have disappeared and others have grown; this is consistent with the Ostwald ripening process.

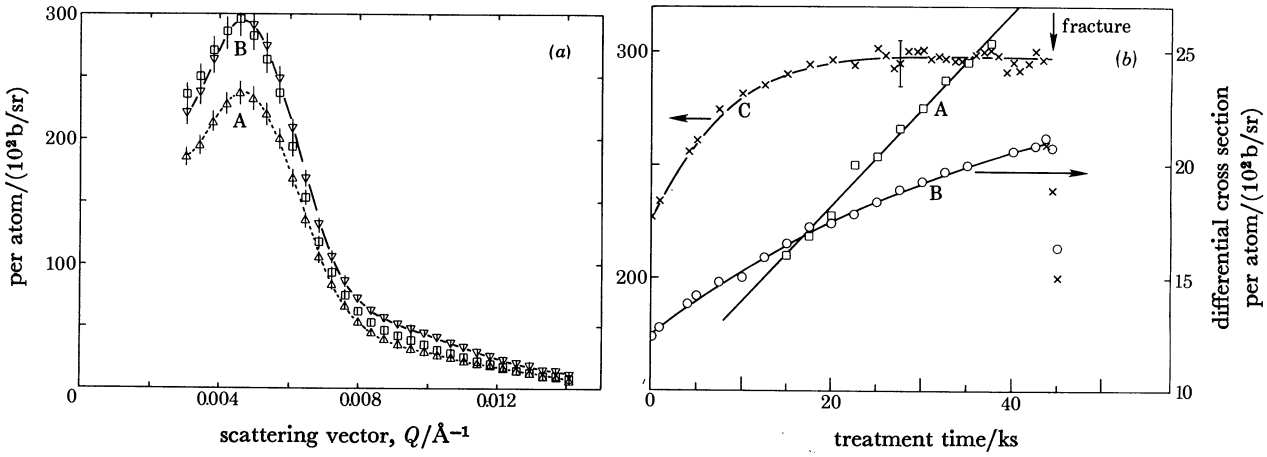

FIGURE 4. (*a*) Nimonic 105 alloy (A) as heat treated and (B) after 13 h *in situ* treatment at 500 MPa and 800 °C. (*b*) Comparison of creep (A) and scattering cross section at a Q of 0.014 Å^{-1} (B) and at a Q of 0.005 Å^{-1} (C).

In the dynamic experiment, we measured the creep and neutron scattering simultaneously and wished to monitor both to the point of rupture. In order to achieve this in the available time we used a higher stress and temperature (500 MPa, 800 °C) but after 13 h these were increased to 550 MPa and 850 °C, after which rupture occurred after 30 min. Adequate statistical accuracy was obtained on measurements lasting 250 s. The creep was monitored by a high-precision electrical transducer fixed to the sample and showed a mean fractional creep rate initially of 0.05% h^{-1}.

The scattering pattern at the beginning of the experiment and just before rupture are shown in figure 4*a*; data taken at $Q = 0.004$ and 0.009 Å^{-1} respectively are compared with the creep rate in figure 4*b*. While in the early stages of creep both the high and low Q correlate with the creep rate, as the rupture point is approached figure 4*b* shows that the creep correlates with the higher Q data. The curves in figure 4*a* show that Q_{max} did not change, unlike the lower temperature–stress experiments. We suggest that in the accelerated stage, as rupture is approached, a further source of scattering in the high Q region develops. One possibility is the formation of microvoids which become the dominant mode of failure in the higher temperature–stress conditions.

Clearly, the process is complicated and further experiments are needed. What has been shown, however, is that these processes may be followed on thick samples by '*in situ*' s.a.n.s.

(c) *Application to irradiated semiconductors*

(i) *Introduction*

When crystals are irradiated with high energy particles, atoms of the crystal are displaced from their normal position. Various point defects (vacancies, interstitials) or small defect complexes (divacancies, di-interstitials, vacancy–impurity complex, interstitial–impurity complex, etc.) may be formed. At one extreme (e.g. bombardment with 0.5 MeV electrons), the recoil energies are small (less than 100 eV, say) and the process is close to threshold. In the other extreme (e.g. fission energy neutrons in a reactor), the recoil energies are *ca.* 0.5 MeV and the energetic knock-on atoms produce *ca.* 1000 further displacements in coming to rest.

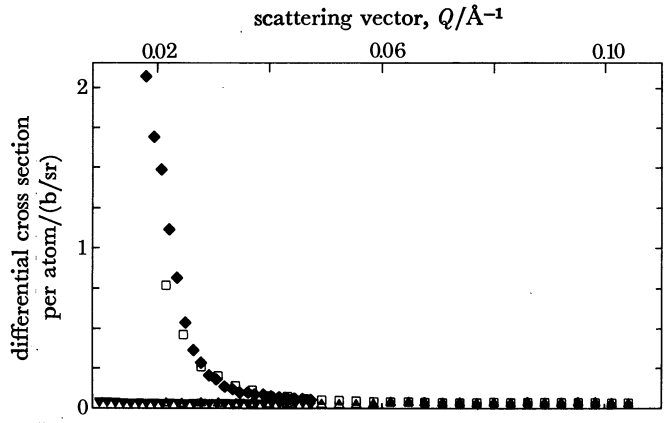

FIGURE 5. The small-angle scattering from irradiated (□, ◆) and unirradiated (△, ▼) GaAs. △, □, 2 m data; ▼, ◆, 5 m data. Irradiation was with 9×10^{19} neutrons/cm^2.

Because of the penetration of the neutron, this damage by energetic knock-on atoms is produced throughout the crystal. However, in a number of semiconductors there is indirect evidence from the electrical and optical properties of the irradiated crystals that at high neutron doses the damage is not uniformly distributed (e.g. silicon (Gossick 1959), gallium arsenide (Coates & Mitchell 1975)). In the present experiments we have used s.a.n.s. to obtain structural information above the defect distribution. If the defects occur in clusters, for example, there should be a density fluctuation that would give rise to s.a.n.s.

(ii) *Gallium arsenide*

Coates & Mitchell (1975) have described the changes in electrical and optical properties that follow the introduction of defects into GaAs by fast neutron irradiation. From the analysis of these results they concluded that the defects were not uniformly distributed. Subsequently Gupta *et al.* (1978) carried out s.a.n.s. measurements.

The s.a.n.s. curves for irradiated and unirradiated crystals are shown in figure 5. There is pronounced small-angle scattering with $R_g \approx 150$ Å. However, the scattering was not isotropic and the scattering pattern for the incident neutron beam along [111] is shown in figure 6.

This pattern has been compared with computations based on (7). The anisotropy in the scattering pattern is that of the Fourier transform of the shape function of the inhomogeneity. Gupta *et al.* (1978) concluded that the fluctuations were ellipsoidal. Further work is in progress concerning both the orientation of the ellipsoids and the method of their production by the radiation damage process.

PHILOSOPHICAL TRANSACTIONS OF THE ROYAL SOCIETY B BIOLOGICAL SCIENCES

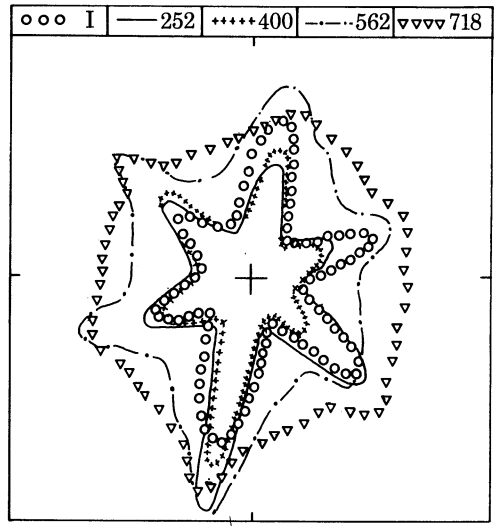

FIGURE 6. The effects of annealing on the anisotropic scattering cross section of irradiated GaAs. (Temperature in degrees Celsius.)

(iii) *Silicon*

Beddoe *et al.* (1979) have measured the s.a.n.s. from fast neutron irradiated ultra-purity polycrystalline silicon obtained from the Dow Corning Corporation. The form of the scattering is shown in figure 7*a* and the corresponding Guinier analysis in figure 7*b*. There seem to be two characteristic sizes associated with the scattering, *ca.* 150 Å dominating the lower Q scattering and *ca.* 50 Å the higher Q.

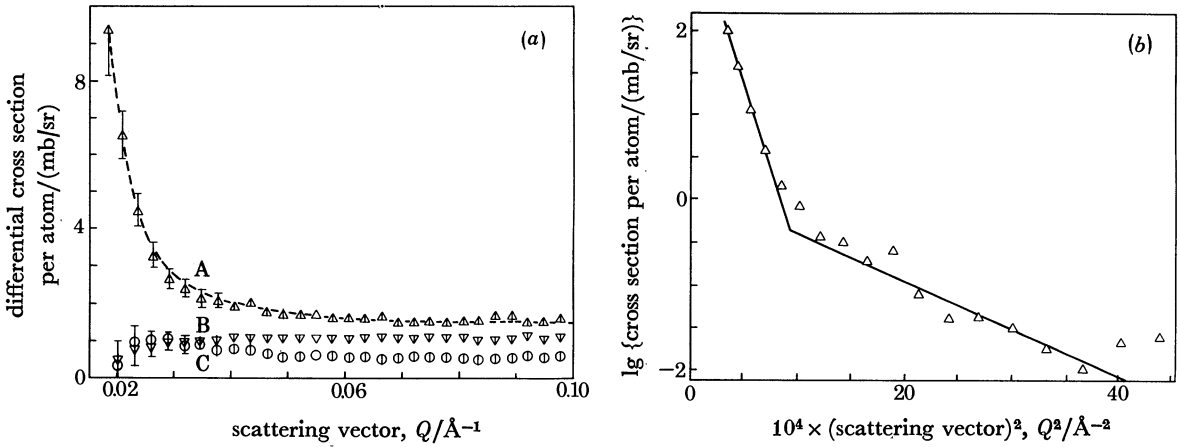

FIGURE 7. (*a*) The irradiation-induced cross section in a polycrystalline silicon sample irradiated with 10^{20} fast neutrons (A); after annealing at 110 °C (B) and after annealing at 700 °C (C). (*b*) Guinier plot of the irradiation induced cross section.

It was possible to study the annealing of this scattering and two of the curves are shown in figure 7*a*. It is clear that substantial annealing occurred at 100 °C throughout the whole Q region, but especially at low Q.

From the e.s.r. measurements of Watkins & Corbett (1965) and the infrared measurements of the 1.7 μm band by Cheng *et al.* (1966), it is known that divacancies are the main defects

in room-temperature electron or neutron irradiated silicon. The divacancies are found to anneal between 100 and 200 °C, the temperature being found by Newman & Totterdell (1975) to be lower for the higher dose irradiations. We propose, therefore, that the s.a.n.s. arises from regions of crystal ($R \approx 150$ Å) containing a high concentration of divacancies. The s.a.n.s. remaining after the 100 °C annealing was further decreased by heating at 700 °C, and this may well be associated with the spectroscopic effects, possibly due to higher vacancy complexes, which were found by Koval *et al.* (1973) and Newman & Totterdell (1975) to anneal at 600 °C.

An interesting aspect of this experiment is the correlation of the structural data (s.a.n.s.) with the spectroscopic data through the annealing characteristic.

4. Diffuse neutron scattering

(*a*) *Theory*

There is a considerable body of theoretical work on the calculation of the form of the diffuse scattering produced by various kinds of defect. The calculations are developments to suit particular purposes of the methods used by James (1948), but can now be carried much further because of the computational power that is available. Good examples of detailed calculations are in the work of Martin (1965), Stewart (1969), Schmatz (1973), Clark *et al.* (1971) and Gupta (1976).†

The theory of diffuse scattering has been reviewed by Schmatz (1973) and discussed extensively by Krivoglaz (1969) in his monograph. These include accounts of the formalisms in which the displacements are described by the virtual forces of the lattice statics developed by Kanzaki (1957). We refer to the convenience of this approach later. It has the disadvantage, apart from the conceptual difficulty of the understanding of fictitious forces as opposed to atomic displacements, of only being applicable for small displacements. There is evidence, however, from the calculations of Larkins & Stoneham (1971) and the experiments of Clark *et al.* (1971), that the displacements of the first two or so shells of atoms around a defect are not necessarily small. In this paper, therefore, we give the essential results of the method that we have used, which provides a description of diffuse scattering in terms of displacements.

We consider an incident beam of amplitude ψ_{i} and wavevector $\boldsymbol{k}_{\mathrm{i}}$ incident on a crystal in a direction $\boldsymbol{\alpha}$ with respect to the crystal axes. The beam scattered by N_{d} (cm^{-3}) defects, each of scattering length b_{d}, at an angle ϕ has amplitude $\psi_{\mathrm{fd}}(\boldsymbol{\alpha}, \phi)$ and wavevector $\boldsymbol{k}_{\mathrm{f}}$. The atoms of the host (N cm^{-3}) have scattering length b; for a vacancy $b_{\mathrm{d}} = -b$, for a substitutional impurity atom (b_{I}), $b_{\mathrm{d}} = b_{\mathrm{I}} - b$, and similarly for small complexes. We describe the normal‡ lattice positions as $\boldsymbol{R}_l$ and suppose that the defects are at various $\boldsymbol{R}_L$. Around each defect (we refer to these as *ca.* R_L) we consider atoms displaced by $\boldsymbol{u}_l$ from their positions $\boldsymbol{R}_{L+l}$ in the reference lattice. The scattered amplitude may then be represented by

$$\psi_{\mathrm{fd}}(\boldsymbol{\alpha}, \phi) = A(\boldsymbol{R}_l) + B(\boldsymbol{R}_L) + C(\boldsymbol{R}_{L+l} + \boldsymbol{u}_l) - D(\boldsymbol{R}_{L+l}), \tag{10}$$

comprising contributions from all reference lattice sites (A), all defects (B), the displaced atoms around each defect (C) and the sites from which these atoms have been displaced (D). From

† Other less detailed calculations are in the work of Antal *et al.* (1958), Sabine *et al.* (1962), Mitchell (1966) and Belson (1968).

‡ It makes little difference for our purposes whether we consider the average lattice of the crystal with defects as the reference or the unperturbed lattice; strictly it should be the former.

PHILOSOPHICAL TRANSACTIONS OF THE ROYAL SOCIETY B BIOLOGICAL SCIENCES

(10) the calculations are straightforward in principle but complicated in practice. The full expression is

$$\psi_{\mathrm{fd}}(\boldsymbol{\alpha}, \phi) = \sum_{l=0}^{N} b\, \mathrm{e}^{-\mathrm{i}\boldsymbol{Q}\cdot\boldsymbol{R}_l} + \sum_{L=0}^{N_\mathrm{d}} \left\{ b_\mathrm{d}\, \mathrm{e}^{-\mathrm{i}\boldsymbol{Q}\cdot\boldsymbol{R}_L} + \sum_{\substack{ca.\,L \\ l\neq L}}^{N} b\, \mathrm{e}^{-\mathrm{i}\boldsymbol{Q}\cdot(\boldsymbol{R}_{L+l}+\boldsymbol{u}_l)} - \sum_{\substack{ca.\,L \\ l\neq L}}^{N} b\, \mathrm{e}^{-\mathrm{i}\boldsymbol{Q}\cdot\boldsymbol{R}_{L+l}} \right\}, \tag{11}$$

which may be simplified to

$$\psi_{\mathrm{fd}}(\boldsymbol{\alpha}, \phi) = \sum_{l=0}^{N} b\, \mathrm{e}^{-\mathrm{i}\boldsymbol{Q}\cdot\boldsymbol{R}_l} + \sum_{L=0}^{N_\mathrm{d}} \mathrm{e}^{-\mathrm{i}\boldsymbol{Q}\cdot\boldsymbol{R}_L} \left\{ b_\mathrm{d} + \sum_{\substack{ca.\,L \\ l\neq L}}^{N} b\, \mathrm{e}^{-\mathrm{i}\boldsymbol{Q}\cdot(\boldsymbol{R}_l+\boldsymbol{u}_l)} - \sum_{\substack{ca.\,L \\ l\neq L}}^{N} b\, \mathrm{e}^{-\mathrm{i}\boldsymbol{Q}\cdot\boldsymbol{R}_l} \right\}. \tag{12}$$

In (12), the term in braces represents the contribution to the scattering of one defect and its associated strain field. The summation over the random sites $\boldsymbol{R}_L$ gives a multiplying factor of $N_\mathrm{d}^{\frac{1}{2}}$ and we have

$$\psi_{\mathrm{fd}}(\boldsymbol{\alpha}, \phi) = \sum_{l=0}^{N} b\, \mathrm{e}^{-\mathrm{i}\boldsymbol{Q}\cdot\boldsymbol{R}_l} + N_\mathrm{d}^{\frac{1}{2}} \left\{ b_\mathrm{d} + \sum_{\substack{ca.\,L \\ l\neq L}}^{N} b\, \mathrm{e}^{-\mathrm{i}\boldsymbol{Q}\cdot(\boldsymbol{R}_l+\boldsymbol{u}_l)} - \sum_{\substack{ca.\,L \\ l\neq L}}^{N} b\, \mathrm{e}^{-\mathrm{i}\boldsymbol{Q}\cdot\boldsymbol{R}_l} \right\}, \tag{13}$$

or, in the form similar to (10),

$$\psi_{\mathrm{fd}}(\boldsymbol{\alpha}, \phi) = \mathscr{A} + N_\mathrm{d}^{\frac{1}{2}}\{\mathscr{B} + \mathscr{C} - \mathscr{D}\}. \tag{14}$$

The differential scattering for a single crystal is $(\mathrm{d}\sigma/\mathrm{d}\Omega)\ (\boldsymbol{\alpha}, \phi) = N^{-1}|\psi_\mathrm{f}\psi_\mathrm{f}^*|$; for a polycrystalline sample this is averaged over all $\boldsymbol{\alpha}$; the total cross section $\sigma(|k_\mathrm{i}|)$ for such a sample is the latter integrated over all ϕ and Ω; and for a single crystal $(\mathrm{d}\sigma/\mathrm{d}\Omega)\ (\boldsymbol{\alpha}, \phi)$ is integrated over all ϕ and Ω to give $\sigma(\boldsymbol{k}_\mathrm{i})$. These quantities are interrelated; in particular it is fairly easily shown that the information for a polycrystalline sample contained by $\mathrm{d}\sigma/\mathrm{d}\Omega$ as a function of ϕ is equivalent to σ as a function of $|k_\mathrm{i}|$, provided $|k_\mathrm{i}| \leqslant \frac{1}{2}\tau_{\min}$, where $\tau_{\min}$ is the minimum reciprocal lattice vector.

To calculate the differential scattering, we consider a matrix whose components are the order of N_d of the relevant terms. We have

	$\mathscr{A}$	$\mathscr{B}$	$\mathscr{C}$	$\mathscr{D}$
$\mathscr{A}^*$	0	$N_\mathrm{d}^{\frac{1}{2}}$	$N_\mathrm{d}^{\frac{1}{2}}$	$-N_\mathrm{d}^{\frac{1}{2}}$
$\mathscr{B}^*$	$N_\mathrm{d}^{\frac{1}{2}}$	N_d	N_d	$-N_\mathrm{d}$
$\mathscr{C}^*$	$N_\mathrm{d}^{\frac{1}{2}}$	N_d	N_d	$-N_\mathrm{d}$
$\mathscr{D}^*$	$-N_\mathrm{d}^{\frac{1}{2}}$	$-N_\mathrm{d}$	$-N_\mathrm{d}$	N_d

For typical defect concentrations we need only consider the terms in N_d, that is, those in the box. The main computation problem, therefore, is dealing with the displacements around each defect.

Away from the defect (say from the third or fourth shells, but this has to be determined empirically) the displacements will be of the form deduced by Eshelby (1956) from continuum theory:

$$u_l = a/|\boldsymbol{R}_l - \boldsymbol{R}_L|^2. \tag{15}$$

The strength and sign of the dilatation has to be assigned. Larkins & Stoneham (1971) and Clark *et al.* (1971) have considered first shell displacements as large as 20%. We have also to allow for displacements of opposite sign in the first two shells (see §4*b*). Some simplifications in computing procedure have been made by Gupta (1976).

The alternative analytical approach has been carried furthest by Schmatz (1973) and this introduces considerable simplifications when *all* the displacements are small. When *all* the

PHILOSOPHICAL TRANSACTIONS OF THE ROYAL SOCIETY B BIOLOGICAL SCIENCES

displacements are *not* small, Schmatz (1973) retains the formalism appropriate to small displacements but introduces a correction term; this may be done exactly but in so doing the same complications re-enter.

In the limit of small displacements,

$$e^{iQ\cdot(R_l+u_l)} \quad \text{becomes} \quad iQu_l\, e^{iQ\cdot R_l},$$

and we may write

$$|\psi_f\psi_f^*| = N_d\,|b_d + b\{iQ\mathscr{F}\{u_l\} + H(u_l)\}|^2, \tag{16}$$

where the Fourier series

$$\mathscr{F}\{u_l\} = \sum_{l=-\infty}^{\infty} u_l\, e^{iQ\cdot R_l}.$$

The correction term $H(u_l)$ if the displacements are not small is

$$H(u_l) = \sum_{l=-\infty}^{\infty} e^{iQ\cdot R_l}\,(e^{iQ\cdot u_l} - 1 - iQu_l). \tag{17}$$

Equation (16), which follows directly from (13), is the definitive equation (47) referred to by Schmatz (1973). For very small Q,

$$H(u_l) \to 0$$

and

$$|\psi_f\psi_f^*| \to N_d b_d^2 \quad \text{or} \quad d\sigma/d\Omega = c_d b_d^2.$$

If the u_1 are small, the scattered intensity is related to the Fourier transform of the displacements, which in turn can be represented by the dynamical matrix of the phonon displacements. When they are not small, the use of (17) involves a physically fictitious correction and we prefer to compute directly from (13). We have used various assumed values of real displacements usually for the first two shells (say 20 atoms) with a continuum equation for subsequent shells. Thus the computation is readily managed for three unknowns: first and second shell displacements and a strength parameter for the continuum theory.

(*b*) *Computational studies*

The effects of relaxation around a defect on the scattering cross section can be calculated by using the expressions derived in the previous section, provided some assumptions are made to determine the positions of the atoms in the radial strain field produced by the defect. In an elastic continuum the amount of relaxation surrounding a point source of dilation is given by (15). For the first neighbour shell various assumed relaxations can be used to determine the value of the strength parameter a. Radial relaxations for subsequent shells are calculated from (15).

An extensive series of such calculations to determine the total cross section were made by Clark *et al.* (1971) for various defects in germanium. The discrimination that can be achieved in the determination of the details of the relaxation field associated with a defect are illustrated by the calculations of the differential cross section arising from various relaxation models associated with a divacancy in a single crystal of silicon (M. R. Baig & R. J. Stewart, personal communication). In these calculations, the relaxations out to the fifth nearest neighbour shell were included, involving a total of 54 atoms. We illustrate the type of effects that it may be possible to observe in the computational results shown in figure 8. Here the first shell is relaxed inwards by 20% and the third, fourth and fifth shells are given inward relaxations of amounts given by (15). The second shell, however, is varied from inward (also given by (15)), to no

PHILOSOPHICAL TRANSACTIONS OF THE ROYAL SOCIETY B BIOLOGICAL SCIENCES

relaxation and to outward relaxation. Such opposite relaxations of second shells of atoms surrounding defects have been shown to occur in lattice calculations involving interatomic force simulations.

The results in figure 8 show that the second shell position considerably influences $(d\sigma/d\Omega)$ for $Q \approx 0.1$, 0.28 and 0.35 Å^{-1}. Such differences should be observable. It is clearly desirable that diffuse scattering measurements are made simultaneously throughout the whole Q region as is now possible with D11 and will be possible with the S.N.S. small-angle scattering instrument.

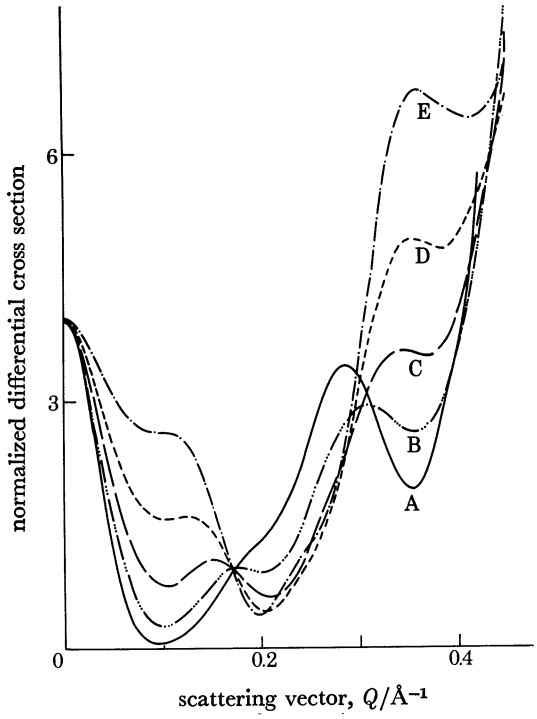

FIGURE 8. Theoretical differential cross section for divacancies in silicon, with the first nearest neighbour atoms relaxed towards the divacancy by 20%. The next four nearest neighbour shells are relaxed according to (15) with the exception of the second nearest neighbours, for which the relaxation is modified. The values of a in (15) for this are: a for curve A, $\frac{1}{2}a$ for B, 0 for C, $-\frac{1}{2}a$ for D and $-a$ for E.

(*c*) *Experiments*

Very little experimental work has so far been carried out. Clark *et al.* (1971) compared the λ dependence of the total cross section with various relaxations around defects in germanium. The most interesting experiment, however, is that of Seitz *et al.* (1975), who measured the diffuse scattering of single crystals of Pb containing 2% and 4% Bi. The experiments show the effects of the relaxation of Pb atoms surrounding the impurity. Calculations for this system have been made by Schumaker *et al.* (1973). The experimental results are in good agreement with a strain of trigonal symmetry. The detailed intensities in the 100, 110, 111 representative triangle are well described by the relaxation model provided that both attractive and repulsive (fictitious – see §4*a*) forces are assumed.

The possibilities of determining these strain effects, about which there is very little information, from diffuse neutron scattering looks extremely promising.

PHILOSOPHICAL TRANSACTIONS OF THE ROYAL SOCIETY B BIOLOGICAL SCIENCES

We should like to thank colleagues who have collaborated with us over a number of years in this work at the University of Reading, A.W.R.E. (Aldermaston) and the Institut Laue-Langevin (Grenoble).

Bibliography (Mitchell & Stewart)

Allen, D. R. 1978 Ph.D. thesis, University of Reading.
Allen, D. R., Epperson, J. E., Gerold, V., Kostorz, G., Messoloras, S. A. & Stewart, R. J. 1976 In *Proc. Conf. on Neutron Scattering* (ORNL Report no. CONF-760601-P1), pp. 102–108.
Allen, D. R., Messoloras, S. A., Stewart, R. J. & Kostorz, G. 1978 *J. appl. Crystallogr.* **11**, 578–580.
Antal, J. J. & Goland, A. N. 1958 *Phys. Rev.* **112**, 103–111.
Beddoe, R. E. 1978 Ph.D. thesis, University of Reading.
Beddoe, R. E., Messoloras, S. A., Mitchell, E. W. J. & Stewart, R. J. 1979 *Inst. Phys. Conf. Ser.* no. 46, pp. 258–266.
Belson, J. 1968 Ph.D. thesis, University of Reading.
Cheng, L. J., Corelli, J. C., Corbett, J. W. & Watkins, G. D. 1966 *Phys. Rev.* **152**, 761–774.
Clark, C. D. & Meardon, B. H. 1972 *Nature, phys. Sci.* **235**, 18–20.
Clark, C. D., Messoloras, S. A., Mitchell, E. W. J. & Stewart, R. J. 1975 *J. appl. Crystallogr.* **8**, 127.
Clark, C. D., Mitchell, E. W. J. & Stewart, R. J. 1971 *Cryst. Lattice Defects* **2**, 105–120.
Coates, R. & Mitchell, E. W. J. 1975 *Adv. Phys.* **24**, 593–644.
Eshelby, J. D. 1956 *Solid State Phys.* **3**, 79–144.
Gerold, V. 1961 *Physica Status Solidi* **1**, 37–49.
Gossick, B. R. 1959 *J. appl. Phys.* **30**, 1214–1218.
Guinier, A. 1959 *Solid State Phys.* **9**, 293–398.
Guinier, A. & Fournet, G. 1955 *Small angle scattering of X-rays*. New York: Wiley.
Gupta, S. 1976 Ph.D. thesis, University of Reading.
Gupta, S., Mitchell, E. W. J., Stewart, R. J. & Kostorz, G. 1978 *Phil. Mag.* A **37**, 227–243.
Hosemann, R. & Bagchi, S. N. 1962 *Direct analysis of diffraction by matter*. Amsterdam: North-Holland.
Ibel, K. 1976 *J. appl. Crystallogr.* **9**, 296–309.
James, R. W. 1948 *Optical principles of the diffraction of X-rays*. London: G. Bell.
Kanzaki, H. 1957 *J. Phys. Chem. Solids* **2**, 24–37.
Kostorz, G. 1979 In *Treatise on materials science and technology* (ed. G. Kostorz), vol. 15, pp. 227–289. New York: Academic Press.
Koval, Y. P., Mordkovich, V. N., Temper, E. M. & Kharchenko, V. A. 1973 *Soviet Phys. Semicond.* **6**, 1152–1155.
Krivoglaz, M. A. 1969 *Theory of X-ray and thermal neutron scattering by real crystals*. New York: Plenum Press.
Larkins, F. P. & Stoneham, A. M. 1971 *J. Phys.* C **4**, 143–163.
Laslaz, G., Kostorz, G., Roth, M., Guyot, P. & Stewart, R. J. 1977 *Physica Status Solidi* a **41**, 577–583.
Martin, D. G. 1965 Ph.D. thesis, University of Reading.
Meardon, B. H. 1970 Ph.D. thesis, University of Reading.
Messoloras, S. A. 1974 Ph.D. thesis, University of Reading.
Miller, R. J. R., Messoloras, S. A., Stewart, R. J. & Kostorz, G. 1978 *J. appl. Crystallogr.* **11**, 583–588.
Mitchell, E. W. J. 1966 *A.E.R.E. Report* no. R5269 230–242. United Kingdom Atomic Energy Authority.
Newman, R. C. & Totterdell, D. H. T. 1975 *J. Phys.* C **8**, 3944–3954.
Porod, G. 1951 *Kolloidzeitschrift* **124**, 83–95.
Powell, M. J. D. 1965 *Comput. J.* **7**, 303–307.
Sabine, T. M., Pryor, A. W. & Hichman, B. S. 1962 *Phil. Mag.* **8**, 43–57.
Schumacher, H., Schmatz, W. & Seitz, F. 1973 *Physica Status Solidi* a **20**, 109–117.
Schmatz, W. 1973 In *Treatise on materials science and technology* (ed. H. Herman), vol. 2, pp. 105–229. New York: Academic Press.
Seitz, E., Schmatz, W., Bauer, G. & Just, W. 1975 *J. appl. Phys.* **8**, 183.
Shull, C. G. & Roess, L. C. 1947 *J. appl. Phys.* **18**, 295–307.
Stewart, R. J. 1969 Ph.D. thesis, University of Reading.
Stewart, R. J. 1978 *The small angle neutron scattering apparatus for the SNS*. Didcot: Rutherford Laboratory.
Walker, C. & Guinier, A. 1953 *Acta metall.* **1**, 568–579.
Watkins, G. D. & Corbett, J. W. 1965 *Phys. Rev.* A **138**, 543–555.

PHILOSOPHICAL TRANSACTIONS OF THE ROYAL SOCIETY B BIOLOGICAL SCIENCES

Discussion

R. J. R. Miller (*Ministry of Defence, Main Building, Whitehall, London, U.K.*). I should like very briefly to describe the small-angle neutron scattering machine at the M.O.D.'s 5 MW reactor Herald at Aldermaston to give context to my remarks. The machine consists of a 3 l H_2–D_2 cold source at 20 K, giving a cold beam of neutrons which are passed through a conventional velocity selector onto the sample, a 4.5 m evacuated flight tube and a multi-detector. The latter is a 128 × 128 element detector made by the C.E.N.G. The velocity selector has a variable resolution of 5–25% and the collimation before the sample will be done by thin-wall Soller collimators. The machine is very much less powerful (two orders of magnitude) than the D11 machine at Grenoble, but there is still a wide range of useful experiments that can be performed.

In particular, measurements on technological samples where differences from the norm are sought can be made. Many of these samples are very powerful scatterers of neutrons at small angles, so that very powerful neutron sources are not absolutely necessary. In addition, the mechanical properties of technologically interesting materials, almost by definition, vary slowly with time so that '*in situ*' experiments, where the sample is subjected to typical operating temperatures, stresses, etc., may need to take many weeks. Such long-term experiments can only be carried out on less powerful machines.

E. W. J. Mitchell. Clearly there are experiments that can usefully be done on medium flux reactors, especially if the long wavelength flux is enhanced by a cold source, as in the example given by Dr Miller. The experiments described in our paper were chosen to illustrate the types of measurements that may be made with the use of high fluxes.

D. J. Cebula (*Rutherford Laboratory, Didcot, Oxon., U.K.*). Many of the scattering patterns presented display marked peaks in the low Q region. These peaks can presumably be attributed to diffraction effects arising from the particle–particle correlations in the sample. Has any attempt been made to separate the structure factor part of the total signal from the single particle factor and thus obtain quantitative information about the radial distribution of particles?

E. W. J. Mitchell. In principle, it is possible to obtain information about the radial distribution function of the particles. However, in practice it is difficult to obtain sufficient data on the low Q side of the maximum. Furthermore, unless the particles are closely of the same size, the higher ripples of the interference function are lost.

PHILOSOPHICAL TRANSACTIONS OF THE ROYAL SOCIETY B BIOLOGICAL SCIENCES